The Astrophysical Journal, 698:786–802, 2009 June 10 doi:10.1088/0004-637X/698/1/786

CHROMOSPHERIC VARIABILITY IN EARLY F-TYPE STARS

Brian L. Rachford[1] and Dillon R. Foight
Department of Physics, Embry-Riddle Aeronautical University, 3700 Willow Creek Road, Prescott, AZ 86301, USA; rachf7ac@erau.edu
Received 2009 February 17; accepted 2009 April 9; published 2009 May 22

ABSTRACT

Using precise measurements of the helium D_3 line, we have searched for statistically significant variations in the strength of chromospheric activity in 13 early F-type stars and two late F-type stars. In two early F-type stars, we find short-term (hours to days) variability based on ∼25 observations over the course of a week. In an additional two cases we find significant differences between observations taken years apart, but we can most likely explain this apparent long-term variation as an artifact of probable short-term variations. The evidence suggests that pure rotational modulation of discrete active regions is not responsible for the short-term variations in the early F-type stars and that either a more global process is at work or we are seeing large number of small active regions spread across the star. In contrast, the two late F-type stars in the sample show strength and/or wavelength variations that are consistent with "solar-type" activity typified by the rotational modulation of active regions. Our results suggest that variability does not cause the wide range in activity levels observed within the early F-type stars.

Key words: stars: abundances – stars: activity – stars: chromospheres

1. INTRODUCTION

Chromospheric variability on rotational timescales has been well demonstrated through a variety of spectral indicators in late F- through K-type stars, due to discrete active regions crossing the visible disk (e.g., Baliunas et al. 1983; Ayres 1999; Frasca et al. 2000; Biazzo et al. 2007). As in the Sun, these active regions are thought to be associated with concentrated magnetic fields. In addition, long-term cycles (years to decades) analogous to the 11 year solar cycle have been found in Sun-like stars (Baliunas et al. 1995).

The situation with regards to chromospheric variability in the early F-type stars is less clear. The standard activity indicators become more difficult to observe and there is uncertainty as to the role of magnetic fields in driving the activity resulting from the very thin near-surface convective regions (e.g., Narain & Ulmschneider 1996; Neff & Simon 2008). Nearly all early F-type stars show at least moderately strong activity, with few if any analogs to the weak activity of the Sun (Simon & Landsman 1991; García López et al. 1993; Rachford 1997) and no apparent dependence on age (Rachford 2000). However, within a narrow temperature range or at a specific age across all early F-type stars, a large activity range exists.

Numerous UV emission lines, which stand out against the weak UV continua of these stars, as well as the optical He I λ5876 (D_3) absorption line have been successfully used as chromospheric activity indicators in the early F-type stars. These indicators have occasionally been used in attempts to search for variability, which is one possible explanation for the activity range in these stars. Ayres (1991) used the *IUE* satellite to observe several UV emission lines in Hertzsprung gap star β Cas in an attempt to find rotational modulation. In 20 spectra, the author measured three lines, Lyα, C II λ1335, and C IV λ1549. The observations of the two carbon lines showed standard deviations 20%–50% larger than the typical measurement uncertainties while the Lyα observations showed standard deviations more than twice as great as the typical measurement uncertainties. However, Lyα measurements are greatly affected by interstellar absorption and geocoronal emission, and in addition the author indicated that the measurement uncertainties may have been underestimated in some cases.

Wolff et al. (1986) observed the D_3 line in μ Vir 12 times, but attributed the spectrum-to-spectrum variation to inaccuracies in the removal of telluric line contamination. Rachford (1998) reported evidence of D_3 variability in relatively low-precision data obtained for two early F-type open cluster stars, one in Coma and the other in Praesepe. Despite very limited temporal coverage, the data suggested short-term variability on time scales of less than 1 day. Finally, Teresova (2005) observed the D_3 line in a variety of late-type stars, including several F-type stars. Teresova reported evidence of short-term D_3 variability in one early F-type star and possible evidence of long-term variability based on comparisons with D_3 results from other authors.

To further explore chromospheric variability in the early F stars, we have undertaken an observing program involving high-precision measurements of D_3 in 15 bright stars. A key component of this study is the uniform processing and analysis of the data, particularly important because we must remove photospheric and telluric lines that contaminate the D_3 line. In addition, we pay careful attention to the uncertainties in our measurements, crucial for quantifying variability. Thus, we describe our procedures in some detail, not only in support of the present work but also for related future studies using a broader data set.

We organize the rest of the paper as follows. In Section 2, we describe the observations and the reduction to one-dimensional spectra. In Section 3, we describe in detail our analysis procedures that yield D_3 line parameters. In Section 4, we give an overview of our stellar sample. In Section 5, we describe the results of our search for short-term D_3 variability. In Section 6, we describe the results of our search for long-term variability. In Section 7, we discuss our results and their implications. Finally, we summarize the paper in Section 8.

[1] Visiting Astronomer, Kitt Peak National Observatory, National Optical Astronomy Observatories, which is operated by the Association of Universities for Research in Astronomy Inc., under cooperative agreement with the National Science Foundation.

Table 1
Observing Runs

Run	Dates (UT)	Wavelengths (Å)
sp95	1995 Feb 2–8	5781–5980
fa95	1995 Nov 28–Dec 6	5781–6844
sp96	1996 Feb 20–29	5552–6928
fa96	1996 Oct 17–22	5781–6243
sp97	1997 Mar 7–14	5781–6243
sp98	1998 May 12–18	5781–6243
fa99	2000 Jan 19–27	5661–6840

2. OBSERVATIONS AND DATA REDUCTION

All data were obtained with the now defunct 0.9 m Coudé Feed Telescope at Kitt Peak National Observatory, using the echelle grating, Camera 5, and the F3KB CCD. We used a 300 μm slit corresponding to 2.1 arcsec projected on the sky and the dispersion was 25 mÅ pixel^{-1} near the D_3 line. Based on measurements of Th–Ar lamp spectra, we obtained 2.8 pixel resolution (70 mÅ, 3.6 km s^{-1}, or $\lambda/\Delta\lambda \approx 85000$). Table 1 gives an overview of the observing runs during which we obtained data.

We used standard routines from the IRAF[2] ECHELLE package for bias subtraction, flat-fielding, scattered light removal, reduction to one-dimensional spectra, continuum normalization, and wavelength calibration. For the latter, we obtained several Th–Ar spectra each night, and by fitting ~30 lines per echelle order, we obtained ~50 m s^{-1} rms uncertainty in the wavelength scale on most nights.

With the large horizontal format of the CCD (3072 pixels), we cover ≈75 Å in each order with about 20% overlap across adjacent orders. To perform spectral fits across a wide wavelength range, we must normalize each echelle order and "stitch" together the adjacent orders. The IRAF CONTINUUM package allowed us to interactively fine tune the continuum fitting to best exclude low-flux points associated with photospheric and telluric lines. Thus, we could use a relatively high polynomial order without distorting the stellar lines. As discussed in Section 3.6, the final measurement of the D_3 line involves a small portion of an echelle order that can be fitted with a low-order continuum.

3. DATA ANALYSIS

3.1. Overview

Precise measurement of the D_3 line or any other spectral line requires that the line be as unaffected as possible by other spectral features. For D_3, adjacent photospheric lines as well as telluric water vapor lines can be serious contaminants. The latter is particularly problematic because it is highly variable. Figure 1 illustrates the problem and demonstrates our ability to correct for these contaminants. As this figure shows, much of the problem lies with the telluric lines superposed on the D_3 line, but it is also important to remove photospheric lines for proper continuum rectification.

We remove the photospheric lines by fitting model spectra to a large portion of our observed spectra to determine stellar rotational velocity and abundances of the relevant chemical elements, and then using this information to generate a model spectrum for the immediate D_3 region. We remove the telluric lines by fitting a model to the observed target spectrum, and then using that information to properly scale a very high signal-to-noise (S/N) telluric template spectrum to match the target spectrum.

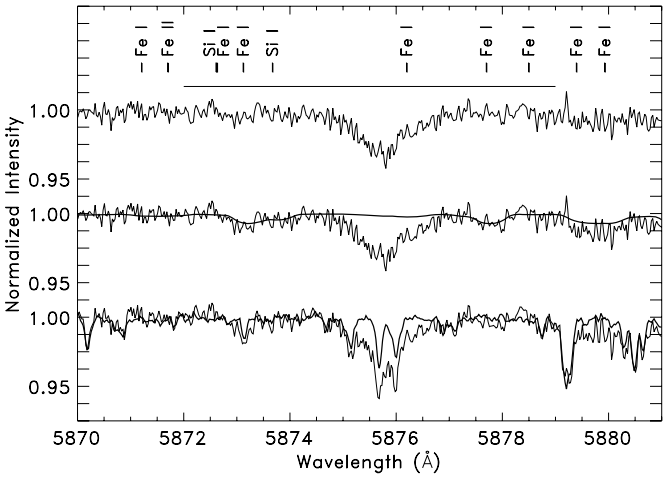

Figure 1. Sample spectrum for the D_3 region showing the sequence of corrections. Bottom: normalized raw spectrum for η Lep with telluric model overplotted (telluric absorption is relatively strong in this spectrum, while photospheric line strengths are about average). Middle: telluric-corrected spectrum with photospheric model overplotted. Top: final D_3 spectrum, with solid line depicting the fit region used to derive line parameters; note that the actual D_3 fit is performed on an unnormalized spectrum.

In both cases, we take advantage of the fact that there are photospheric and telluric lines in other portions of the spectrum that are stronger than the lines that must be removed from the D_3 vicinity. Thus, the absolute errors in the photospheric and telluric fits are minimized when removing the weaker lines. Once we have removed the contaminating photospheric and telluric lines, it is in principle a simple matter to measure the remaining D_3 line. In the following sections, we describe the entire process in more detail.

3.2. Synthetic Spectral Fitting

We synthesized spectra with the SPECTRUM program (Gray & Corbally 1994), which requires as inputs a line list and a stellar atmospheric model. For the former, we started with the list of solar lines given by Thevenin (1990), supplemented with Robert Kurucz's on-line lists.[3] We synthesized each line individually for both a solar model ($T_{\rm eff} = 5777$ K and $\log g = 4.4377$) and a late A star ($T_{\rm eff} = 8000$ K and $\log g = 4.0$) to see which lines are important in the temperature range of our data, deleting lines with equivalent widths less than 0.1 mÅ in both models. Through an iterative process, we adjusted some of the oscillator strengths to match our own solar spectrum (the lunar disk observed with the same equipment as the stellar observations). Except for a small percentage of lines in the Kurucz list that were grossly in error, most differences were small, and we only adjusted lines that clearly did not match our observed spectrum. For these adjustments, we used the solar abundances tabulated by Gray (1992, p 319, see references within).

We assume that the photospheric lines remain constant in the stars, so to determine the elemental abundances we optimized the S/N to provide a "key" spectrum for each star. Target information will be given in Section 4, but for stars with a small number of observations, we chose the one with the highest S/N

[2] IRAF is distributed by the National Optical Astronomy Observatory, which is operated by AURA Inc., under cooperative agreement with the National Science Foundation.

[3] http://cfaku5.harvard.edu/

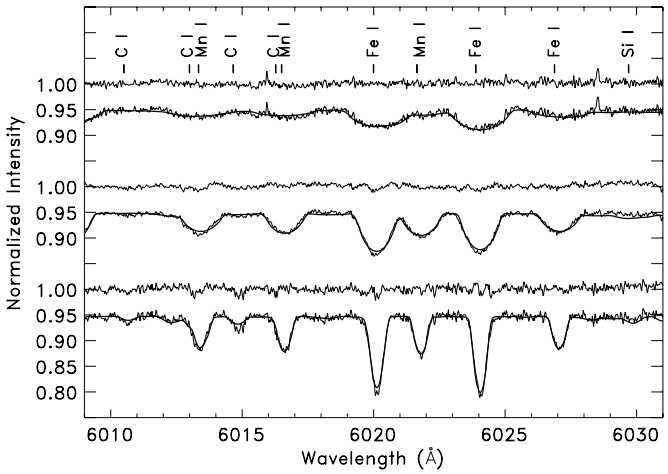

Figure 2. Comparison of observed (thin lines) and synthetic (thick lines) spectra for a range of rotational broadening for a portion of the 6007–6200 Å fit range. Residuals in the sense observed divided by synthetic are given above each spectrum. From top to bottom, stars are ρ Gem ($v \sin i = 58.3$ km s^{-1}), 18 Boo (38.9 km s^{-1}), and η Lep (17.4 km s^{-1}). Species identifications are given for the strongest lines.

(excluding data from a run with limited wavelength coverage), and for the stars that were observed several times in a night we co-added all spectra from a single night to give a very high S/N key spectrum. We chose the range 6007–6200 Å to maximize the number of elements we could fit and minimize the presence of telluric lines as this latter correction is best determined with accurate knowledge of the photospheric spectrum.

For the key fits, we used the Levenberg-Marquardt nonlinear least squares method (i.e., the "CURFIT" algorithm from Bevington & Robinson 1992). The free parameters in the fits are the zero-point wavelength shift, microturbulent speed, $v \sin i$, and the logarithmic elemental abundances. In addition to rotational broadening, we include instrumental broadening (a Gaussian with an FWHM of ∼70 mÅ based on the Th–Ar lines used for wavelength calibration) and macroturbulent broadening (a polynomial approximation to the radial-tangential macroturbulence function given by Gray (1988, p 1–18) corresponding to 5 km s^{-1} for the F-type stars). Both additional broadenings are generally small compared to $v \sin i$ for our stellar sample. Figure 2 shows a portion of the key fit region for three of our stars.

We only perform the key fit for one spectrum (or one summed spectrum) for a star and use that information to produce a model spectrum for the D_3 area in all spectra. However, we need an accurate wavelength shift to properly apply this model spectrum to each additional spectrum. Thus, we fit the 5845–5865 Å region, which contains enough lines to provide an accurate shift and is in the same original echelle order as D_3, eliminating possible differences between the wavelength solutions in different orders. However, in this region only calcium, iron, and barium have strong enough lines for abundance determinations. We perform this fit for all spectra using the downhill simplex method (the "AMOEBA" algorithm from Press et al. 2000), which we prefer over "CURFIT" when fitting poorly known parameters. The information from these fits can then be used to provide good guesses for the parameters of the key fit for each star, which includes more elements as discussed below.

We use the wavelength shift from the 5845–5865 Å region to derive heliocentric velocities using the IRAF RVCORRECT procedure. We report these velocities along with the D_3 line parameters, primarily as a rough indicator of binarity. We do not report formal uncertainties for each of these measurements as the "AMEOBA" algorithm does not report them, but they typically range from about 0.2–0.3 km s^{-1} for the stars with the smallest $v \sin i$ to as much as 1–2 km s^{-1} for the stars with the largest $v \sin i$. These uncertainties are far smaller than those for the D_3 central wavelengths that we report and are thus not a significant source of error for these wavelengths.

Table 2
Solar Abundance Fit

Value	Present	Gray[a]	GS[b]
log A(C)	8.52	8.66	8.52
log A(O)	8.94	8.91	8.83
log A(Si)	7.61	7.64	7.55
log A(S)	7.21	7.23	7.33
log A(Ca)	6.37	6.34	6.36
log A(Mn)	5.56	5.42	5.39
log A(Fe)	7.54	7.59	7.50
log A(Ni)	6.31	6.27	6.25
log A(Ba)	2.19	2.13	2.13

Notes.
[a]Values from Gray (1992).
[b]Values from Grevesse & Sauval (1998).

In addition to the two fitted spectral regions, we must model the 5880–5904 Å range (also in the same original echelle order as D_3) to properly determine the strength of telluric absorption and the 5865–5885 Å region to remove the contaminating lines from the D_3 vicinity. The net result is that we end up modeling the entire range from 5845 to 5904 Å.

We used 72-level Kurucz (1992) stellar models, originally generated on a temperature grid with spacing 250 K and a log g spacing of 0.5 dex. For our fits, we interpolated the models to provide 125 K and 0.1 dex spacing, respectively, for temperature and gravity. The models assume a depth-independent microturbulence of 2.0 km s^{-1}, a reasonable choice for our stars as the actual derived microturbulences from the model fits are in the range 1–4 km s^{-1}.

We used the software developed by Napiwotzki et al. (1993) to derive the effective temperature and surface gravity from *uvbyβ* photometry taken from the Hauck & Mermilliod (1998) catalog. We then rounded these values to match our Kurucz model grid and used that specific model for a particular star. The Napiwotzki et al. (1993) code also calculated stellar radii based a relationship between the Strömgrem photometry and surface brightness derived by Moon (1984), and a slightly modified version of the Barnes & Evans (1978) relationship among the surface brightness, absolute magnitude, and radius. However, we used *Hipparcos* absolute magnitudes instead of those calculated by the Napiwotzki et al. (1993) code. The stellar radii in turn allow us to calculate the projected rotational periods for the stars.

In the key fits, we allowed the abundances of up to nine elements to vary, including the elements that are most likely to interfere with D_3. These elements are listed in Table 2, which also gives our derived solar abundances, discussed in Section 3.4. For our early F-type stars we could not always reliably determine abundances for all nine elements, so we only report values for the five elements most accurately fitted in all 15 stars. This still includes all species that significantly interfere with the D_3 region in F-type stars. Weaker lines from approximately 20 additional elements were modeled using solar abundances. The SPECTRUM program calculates model spectra using the local

Table 3
Procyon Abundance Fits

Value	6625[a]	6750[a]	VM[b]
ξ_t (km s^{-1})	1.85	2.02	1.9
log A(C)	8.50	8.47	8.67
log A(O)	8.87	8.77	8.75
log A(Si)	7.64	7.67	7.58
log A(S)	7.11	7.08	
log A(Ca)	6.43	6.45	6.31
log A(Mn)	5.29	5.33	
log A(Fe)	7.56	7.58	7.48
log A(Ni)	6.27	6.33	6.24
log A(Ba)	2.36	2.30	2.16

Notes.
[a]Stellar model temperature
[b]Values from Varenne & Monier (1999) with a 6696 K model.

thermodynamic equilibrium (LTE) assumption. In the early F stars, this is a reasonable approximation for the weak to moderate line strengths we cover.

3.3. Verification of the Spectral Modeling

We tested our fitting procedures on spectra of the Sun (the lunar disk) and α CMi (Procyon; F5 IV–V), one of our D_3 program stars. Since we used the solar spectrum to adjust the gf factors, we would expect the fit to this spectrum to be an excellent match to other studies and it is. Table 2 shows the results of the solar fit for a spectrum with an S/N $\approx$ 500, using a model with $T_{\rm eff} = 5770$ K and log $g = 4.4377$. We found a reasonable microturbulent velocity, $\xi_t = 1.04$ km s^{-1}. The rotational broadening, $v \sin i = 2.13$ km s^{-1}, closely matches the solar equatorial rotation speed of 1.98 km s^{-1}.

Table 3 lists similar data for a spectrum of Procyon with an S/N $\approx$ 300, using a model with $T_{\rm eff} = 6625$ K and log $g = 4.1$. We found $\xi_t = 1.85$ km s^{-1} and $v \sin i = 5.78$ km s^{-1}. These values compare well with other studies; for example, $\xi_t = 2.1$ km s^{-1} by Steffen (1985) from a curve-of-growth analysis and $\xi_t = 1.9$ km s^{-1} by Varenne & Monier (1999) via a similar procedure to ours. Fekel (1997) derived $v \sin i = 4.9$ km s^{-1} and Varenne & Monier (1999) found $v \sin i = 7$ km s^{-1}.

Varenne & Monier (1999) used a model with $T_{\rm eff} = 6696$ K, so to provide a further comparison to our fit, we also performed a fit with $T_{\rm eff} = 6750$ K. This choice brackets the Varenne & Monier (1999) fit with the two most similar models from our grid, and we give the results of both of our fits in Table 3. Additionally, this provides an estimate of the uncertainties in our quoted abundances based on the temperature uncertainty, which Napiwotzki et al. (1993) reported as about 2.5% (~160–180 K) in the temperature range covered by our sample. We see that the abundance uncertainties resulting from the temperature calibration are less than 0.1 dex for the five elements reported for the rest of our sample.

3.4. Telluric Fit

Our procedure for removing telluric water vapor lines is essentially identical to that used in previous papers (Rachford 1998, 2000), so we only give a brief overview here.

Lundström et al. (1991) catalogued the telluric water vapor lines in the range 5868–5917 Å, which accounts for virtually all telluric absorption in this wavelength range. The strongest telluric lines within this range are near the sodium D lines, which were covered by the same echelle order as D_3 in our spectra. With $v \sin i$ and wavelength shifts known from the 5845–5865 Å synthetic spectral fits, we generated an approximate synthetic photospheric spectrum for the range 5884–5904 Å to flag pixels that are significantly affected by photospheric lines and totally exclude them from the telluric model fit. We then fitted the telluric model to the remaining pixels based on the line catalog. Since the water vapor lines scale together, this gives one parameter describing the strength of the lines for that exposure.

We produced a very high S/N template of the telluric spectrum by observing a rapidly rotating, unreddened hot star (Regulus) and using the CONTINUUM routine in IRAF to "flatten" the few shallow photospheric lines. We scaled the template based on the telluric line strength in each target spectrum derived from the model fits, and this scaled template provides the telluric removal. By using this technique, we avoided issues with minor imperfections in the modeling of the weak telluric lines near D_3 since we divided through an actual observed spectrum instead of the model.

3.5. Final Processing

After dividing the target spectrum by the photospheric model and the scaled telluric spectrum, we are left with a spectrum that should only contain D_3 absorption. As with the telluric correction, our techniques are similar to those used in previous work (Rachford 1998, 2000). One potential problem with the construction of the original target spectra is that we must use a relatively high-order polynomial fit to normalize each order of the spectrum, mostly due to the echelle blaze function. While this works well for the spectrum as a whole, there is the risk of small differences from spectrum to spectrum due to the variability of the telluric lines and putative variability in the D_3 line, which may change the exact pixels that are included in the continuum fit. For instance, more pixels may be excluded in the D_3 vicinity if the telluric and D_3 absorption are strong. While we did not see any obvious problems in the normalized spectra, we wanted to be conservative in our search for variability. The original continuum can accurately be fitted with a third-order polynomial in the narrow range around D_3; thus, we applied the photospheric and telluric corrections to the unnormalized spectra.

The D_3 line is typically broadened in excess of the stellar $v \sin i$ (Rachford 2000). Thus, while the observed D_3 profiles are not simply Gaussian nor the $v \sin i$ "bowl" function, at the level of precision of our spectra a Gaussian provides a good match to the profiles. Importantly, this gives us an analytic fitting function for which it is easy to generate formal uncertainties in our derived equivalent widths, crucial for assessing variability. Thus, we performed a seven-parameter fit for each spectrum using the CURFIT routine: central wavelength (λ_0), Gaussian width (σ), Gaussian depth (d), and a third-order continuum. The equivalent width of a Gaussian absorption profile in a normalized spectrum is then simply

$$W_\lambda = \sqrt{2\pi}\sigma d \quad (1)$$

with the final uncertainty in equivalent width calculated with standard error propagation techniques based on the formal uncertainties in σ and d.

3.6. Errors

To assess the existence of variability, we must be certain that the uncertainties on the individual D_3 measurements are accurately determined. To verify that the uncertainties reported by the fitting routine were correct, we performed Monte Carlo

Table 4
Adopted Stellar Parameters

Star Number	Name	HD	V^a	$B-V^a$	MK Type[a]	Gray[b]	T_{eff}[c] (K)	log g[c] (log cm s^{-2})
1	β Cas	432	2.28	0.380	F2 III–IV	F2 III	6877	3.43
2	9 Aur	32537	4.98	0.343	F0 V	F2 V	7023	4.07
3	η Lep	40136	3.71	0.337	F1 III	F1 V	7117	4.21
4	ρ Gem	58946	4.16	0.320	F0 V	F1 V	6943	4.05
5	α CMi	61421	0.40	0.432	F5 IV–V	F5 IV–V	6618	4.05
6	χ Leo	96097	4.62	0.332	F2 III–IV	F2 III	7086	3.91
7	α Crv	105452	4.02	0.334	F2 III–IV	F0 IV–V	6961	4.21
8	18 Boo	125451	5.41	0.385	F5 IV	F3 V	6739	4.37
9	θ Boo	126660	4.04	0.497	F7 V	F7 V	6371	4.29
10	σ Boo	128167	4.47	0.364	F2 V	F4 V	6739	4.37
11	μ Vir	129502	3.87	0.385	F2 III	F2 V	6805	4.24
12	μ^1 Boo	137391	4.31	0.309	F2 IVa	F0 IV	7253	4.00
13	σ Ser	147449	4.82	0.338	F0 V	F1 IV–V	7019	4.03
14	HR 6237	151613	4.84	0.375	F2 V	F2 V	6722	4.16
15	ξ Oph	156987	4.39	0.394	F1 III–IV	F2 V	6723	4.24

Notes.
[a]Values taken from the Hipparcos Catalog (ESA 1997).
[b]Uniform spectral types from Gray & Garrison (1989) and Gray et al. (2001, 2003).
[c]Calculated from Strömgren photometry as described in Section 3.2.

simulations whereby we generated "perfect" D_3 profiles (plus continuum) that matched the results of fits for several stellar spectra. Then we added a large number of random noise vectors to each profile corresponding to the measured S/N of the original spectrum. We then fitted these simulated noisy profiles in the same way as the actual data.

We found that the simulated profiles produced D_3 equivalent widths with uncertainties and standard deviations within 15% of the originally derived values for that spectrum, while the mean equivalent widths of the simulated lines provided nearly exact matches to the actual lines. The results for the central wavelengths and line widths were similar, and indicate that we are not strongly over or underestimating the uncertainties on the individual measurements we report. However, given the relatively small sample sizes, a 15% underestimate of the uncertainties is sometimes enough to significantly affect the interpretation of the results and this will be discussed in more detail in Section 5.1. We mostly attribute the small differences between the actual spectra and the simulations to slight inaccuracies in the telluric and photospheric line removals, and slight differences between the true shape of the observed D_3 lines and a Gaussian.

4. TARGET SELECTION

With the exception of four stars that were extensively observed throughout a specific observing run, most of the observations were taken during nonoptimal observing conditions when we could not observe fainter targets, that is, light to moderate cloudiness or twilight. Thus, we were limited to stars with $V \lesssim 5$. In addition, the weak D_3 line becomes much more difficult to detect with large rotational broadening, so we limited the sample to $v \sin i \lesssim 100$ km s^{-1}. Our goal was to obtain continuum S/N ratios around 200–300, yielding a D_3 equivalent width precision of about 5%–10% for targets with "normal" line strengths; this goal was not achieved in all cases.

Table 4 lists the program stars along with pertinent photometric and spectroscopic data. In addition to data from the *Hipparcos Catalog* (ESA 1997), we also quote a more uniform set of

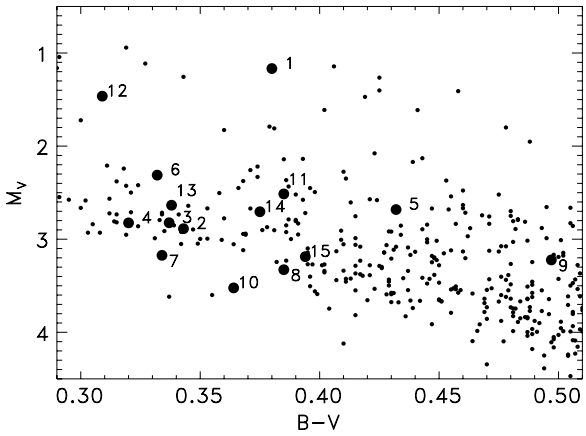

Figure 3. Color–magnitude diagram for stars with *Hipparcos* parallax greater than 25 mas. Program stars are numbered to correspond to Tables 4 and 5.

modern spectral types that provide a much better match to our effective temperatures and surface gravities calculated as described in Section 3.2. Figure 3 gives the positions of each star in a color–magnitude diagram of nearby stars observed by *Hipparcos*. In Table 5, we give the results of our synthetic spectral fits, including microturbulence, rotational velocity, rotational period, and elemental abundances. Our sample can be broadly described as ranging from one-half solar metallicity to full solar metallicity, and our [Fe/H] values agree well with previous measurements.

We had particular reasons for observing two of the four stars for which we investigated short-term variability. We observed 18 Boo due to highly discrepant literature values of the D_3 equivalent width (40 mÅ from Wolff et al. 1986 and 10 ± 5 mÅ from García López et al. 1993). In addition, as discussed in Section 1, μ Vir has already been the subject of a search for D_3 variability. Although our observations were made before the Teresova (2005) study, there are several additional targets in common between our studies.

We have reported D_3 equivalent widths for nine of these stars in a previous work (Rachford 1997). We reanalyzed those spectra for the present study to provide a uniform comparison with the newer observations. In particular, our photospheric fitting and modeling procedures have improved by determining specific abundances for each element for each star, and we model the D_3 lines as Gaussians in the present work as opposed to a wavelength-by-wavelength summation. Our present equivalent widths are generally slightly smaller than the previously reported values, which we mostly attribute to better photospheric line removal, but otherwise the agreement is reasonable. We emphasize that it is somewhat difficult to precisely compare sets of D_3 measurements that have not been processed in exactly the same way due to the telluric and photospheric line removals.

5. SHORT-TERM VARIABILITY

5.1. Overall Results and Statistical Methods

In Tables 6–9, we give observing information and resulting D_3 parameters for the 100 spectra of four stars we used for the investigation of short-term variability, including a few spectra taken to search for long-term variability which will be discussed in Section 6.2. The S/N was determined in the vicinity of the D_3 line, but varies somewhat across the overall spectrum. We also give heliocentric radial velocities, which illustrate that we

Table 5
Synthetic Spectral Fit Results

Star	Name	ξ_t (km s^{-1})	$v \sin i$ (km s^{-1})	$R/R_\odot$[a]	$P/\sin i$[a] (days)	[Si/H]	[S/H]	[Ca/H]	[Ni/H]	[Fe/H]	[Fe/H]$_{\rm lit}$	Ref.
1	β Cas	3.8	70.1	3.43	2.48	−0.25	−0.13	−0.15	−0.42	−0.14		
2	9 Aur	1.9	21.0	1.56	3.76	−0.22	−0.29	−0.02	−0.26	−0.12	−0.20	1[b]
3	η Lep	2.2	17.4	1.62	4.71	−0.05	−0.12	0.10	−0.10	0.00	−0.05	1[b]
4	ρ Gem	2.3	58.3	1.60	1.39	−0.40	−0.32	−0.13	−0.43	−0.27		
5	α CMi	1.9	5.3	1.94	18.52	0.03	−0.10	0.06	−0.04	0.02	−0.02	2[b]
6	χ Leo	3.4	27.5	1.99	3.66	−0.12	−0.11	0.22	0.05	0.04		
7	α Crv	1.8	27.3	1.36	2.52	−0.20	−0.16	−0.06	−0.30	−0.12		
8	18 Boo	1.7	38.9	1.42	1.85	−0.02	0.00	0.01	−0.09	−0.02	−0.02	3
9	θ Boo	1.1	31.8	1.76	2.81	−0.02	−0.03	0.01	−0.07	−0.02	−0.05	4
10	σ Boo	1.5	9.0	1.26	7.09	−0.34	−0.44	−0.26	−0.47	−0.32	−0.41	5[b]
11	μ Vir	2.0	45.8	1.99	2.20	−0.21	−0.18	−0.13	−0.27	−0.17		
12	μ^1 Boo	3.3	82.3	2.93	1.80	−0.15	0.07	−0.04	−0.42	−0.03		
13	σ Ser	3.0	75.8	1.75	1.16	−0.15	0.12	−0.13	−0.20	−0.04		
14	HR 6237	2.0	47.3	1.86	1.99	−0.34	−0.18	−0.21	−0.43	−0.22		
15	ξ Oph	1.7	20.5	1.45	3.57	−0.22	−0.21	−0.10	−0.31	−0.17	−0.13	6

Notes.
(1) Burkhart & Coupry (1991); (2) Varenne & Monier (1999); (3) Boesgaard et al. (1988); (4) Balachandran (1990); (5) Edvardsson et al. (1993); (6) Edvardsson et al. (1984).
[a]Not an observed quantity; calculated as described in Section 3.2.
[b]Other similar measurements are referenced in the Cayrel de Strobel et al. (1997) catalog of [Fe/H] values.

Table 6
D_3 Observations for ρ Gem

N	Run[a]	JD–2400000	S/N (pixel^{-1})	RV (km s^{-1})	W_λ (mÅ)	λ_0 (Å)	FWHM (km s^{-1})
1	sp95	49754.5677	170	−5.12	21.7 ± 3.0	5875.760 ± 0.054	69 ± 7
2	sp96	50137.8234	130	−5.94	24.9 ± 5.0	5875.715 ± 0.082	83 ± 13
3	sp97	50514.6102	191	−5.43	32.6 ± 3.7	5875.819 ± 0.047	88 ± 8
4	sp97	50514.8189	167	−4.76	33.8 ± 4.1	5875.779 ± 0.051	86 ± 8
5	sp97	50515.6139	113	−5.04	32.6 ± 6.3	5875.671 ± 0.084	91 ± 14
6	sp97	50515.7910	279	−4.10	28.7 ± 2.2	5875.717 ± 0.031	78 ± 5
7	sp97	50516.5837	186	−5.52	30.0 ± 3.3	5875.845 ± 0.044	79 ± 7
8	sp97	50516.7915	192	−4.49	33.7 ± 3.9	5875.729 ± 0.053	96 ± 9
9	sp97	50517.5834	195	−5.52	30.0 ± 3.3	5875.898 ± 0.046	83 ± 7
10	sp97	50517.7897	183	−5.17	22.8 ± 2.8	5875.801 ± 0.043	64 ± 6
11	sp97	50518.5817	155	−5.05	32.8 ± 3.9	5875.738 ± 0.047	76 ± 7
12	sp97	50518.7844	157	−5.40	34.5 ± 4.4	5875.780 ± 0.056	89 ± 9
13	sp97	50519.5822	162	−4.15	40.1 ± 4.2	5875.834 ± 0.058	104 ± 9
14	sp97	50519.7998	182	−4.51	41.0 ± 4.3	5875.673 ± 0.046	97 ± 8
15	sp97	50520.5844	196	−4.62	31.3 ± 2.9	5875.795 ± 0.043	83 ± 6
16	sp97	50520.7993	191	−4.96	35.3 ± 4.5	5875.746 ± 0.057	104 ± 10
17	sp97	50521.5959	221	−5.07	33.4 ± 3.2	5875.841 ± 0.043	93 ± 7
18	sp97	50521.8052	147	−4.56	29.8 ± 4.9	5875.665 ± 0.075	95 ± 12
19	sp98	50951.6176	173	−3.68	34.1 ± 3.5	5875.652 ± 0.051	90 ± 7
20	fa99	51562.6578	98	−4.34	23.0 ± 4.9	5875.695 ± 0.071	60 ± 10

Note.
[a]See Table 1 for observing run information.

do not see significant radial velocity variability for these stars. We have numbered the spectra in the tables so we can refer to them individually in further discussion. In all cases, we have also listed the observing run for each observation using the same notation as Table 1 to provide a simpler context for the timing of the observations than the Julian Dates.

We give the central wavelengths of the D_3 lines in the rest frame of the star, based on the photospheric line fits in the 5845–5865 Å range. The reported uncertainties do not explicitly include the wavelength uncertainty of the photospheric fits or possible run-to-run differences in the wavelength solutions, but these errors are typically much smaller than the errors in the D_3 fits. For convenience, we have converted the Gaussian linewidths into the FWHM expressed in km s^{-1}, which can then be compared with $v \sin i$ for the star.

To explore the existence of short-term variability, we begin by calculating various statistics on the measurements of the equivalent width, central wavelength, and linewidth. Table 10 gives a summary of these values. For each quantity, we have tabulated the weighted mean, the weighted standard deviation, and the mean uncertainty of the individual measurements. We chose the mean uncertainty instead of the median uncertainty because the mean was usually slightly larger, giving a slightly

Table 7
D_3 Observations for θ Boo

Star	Run[a]	JD–2400000	S/N (pixel^{-1})	RV (km s^{-1})	W_λ (mÅ)	λ_0 (Å)	FWHM (km s^{-1})
1	sp95	49751.0282	189	−9.96	37.1 ± 2.3	5875.777 ± 0.019	52.2 ± 2.5
2	sp95	49751.0366	181	−10.24	40.5 ± 2.8	5875.671 ± 0.019	56.3 ± 3.0
3	sp97	50518.0140	196	−9.86	42.7 ± 2.7	5875.713 ± 0.017	55.1 ± 2.6
4	sp97	50518.8916	176	−10.03	41.8 ± 2.5	5875.764 ± 0.019	54.0 ± 2.5
5	sp97	50519.0280	185	−10.45	40.8 ± 2.6	5875.757 ± 0.018	54.2 ± 2.6
6	sp97	50519.8902	201	−10.25	40.7 ± 2.7	5875.661 ± 0.018	55.8 ± 2.9
7	sp97	50521.0371	209	−10.19	41.0 ± 2.4	5875.672 ± 0.015	51.8 ± 2.4
8	sp97	50521.8947	215	−10.48	38.1 ± 2.4	5875.719 ± 0.016	52.8 ± 2.5
9	sp97	50522.0147	237	−10.61	42.8 ± 2.3	5875.721 ± 0.015	56.9 ± 2.4
10	sp98	50945.6186	227	−10.19	34.5 ± 2.2	5875.722 ± 0.017	51.8 ± 2.5
11	sp98	50945.9428	196	−10.34	35.4 ± 2.2	5875.702 ± 0.018	51.5 ± 2.4
12	sp98	50946.6136	168	−10.32	33.0 ± 2.9	5875.708 ± 0.024	52.4 ± 3.7
13	sp98	50946.8060	116	−10.37	35.3 ± 4.3	5875.630 ± 0.032	52.4 ± 5.1
14	sp98	50948.6099	203	−10.94	32.5 ± 2.1	5875.756 ± 0.021	53.4 ± 2.8
15	sp98	50948.7982	244	−9.90	37.8 ± 2.3	5875.690 ± 0.017	58.7 ± 2.9
16	sp98	50948.9714	222	−9.93	34.1 ± 2.4	5875.741 ± 0.019	55.4 ± 3.0
17	sp98	50949.6164	224	−10.64	27.0 ± 1.8	5875.707 ± 0.019	48.2 ± 2.4
18	sp98	50949.8087	229	−10.64	36.5 ± 2.3	5875.685 ± 0.017	55.6 ± 2.8
19	sp98	50949.9499	91	−11.43	35.1 ± 4.6	5875.705 ± 0.039	50.5 ± 5.2
20	sp98	50950.6263	134	−10.27	32.4 ± 3.0	5875.670 ± 0.027	47.9 ± 3.5
21	sp98	50951.9703	228	−10.02	32.5 ± 1.8	5875.659 ± 0.017	50.6 ± 2.3
22	fa99	51563.0687	163	−9.71	37.2 ± 3.2	5875.691 ± 0.023	55.3 ± 3.7

Note.
[a]See Table 1 for observing run information.

Table 8
D_3 Observations for μ Vir

N	Run[a]	JD–2400000	S/N (pixel^{-1})	RV (km s^{-1})	W_λ (mÅ)	λ_0 (Å)	FWHM (km s^{-1})
1	fa95	50056.0422	174	4.57	28.9 ± 2.6	5875.694 ± 0.029	55 ± 4
2	sp97	50519.8754	216	3.37	28.8 ± 2.2	5875.785 ± 0.029	64 ± 4
3	sp98	50945.6358	201	2.57	27.1 ± 2.8	5875.885 ± 0.041	74 ± 6
4	sp98	50945.6910	181	2.46	25.4 ± 3.0	5875.759 ± 0.046	71 ± 7
5	sp98	50945.7477	198	2.84	21.9 ± 3.0	5875.740 ± 0.057	77 ± 8
6	sp98	50945.9259	163	2.68	22.5 ± 3.1	5875.718 ± 0.049	64 ± 7
7	sp98	50946.6285	150	3.00	33.2 ± 4.1	5875.613 ± 0.054	83 ± 8
8	sp98	50946.6822	146	2.55	27.7 ± 4.3	5875.823 ± 0.068	85 ± 11
9	sp98	50946.7441	164	3.06	28.1 ± 3.3	5875.843 ± 0.045	71 ± 7
10	sp98	50947.9247	213	2.71	28.6 ± 2.8	5875.608 ± 0.044	85 ± 7
11	sp98	50948.6318	236	2.57	29.3 ± 2.3	5875.727 ± 0.030	70 ± 4
12	sp98	50948.6841	231	2.54	31.6 ± 2.8	5875.896 ± 0.039	87 ± 6
13	sp98	50948.7387	245	3.08	30.2 ± 2.3	5875.773 ± 0.031	76 ± 5
14	sp98	50948.8129	261	3.28	36.5 ± 2.3	5875.777 ± 0.028	80 ± 4
15	sp98	50948.8647	262	3.32	35.0 ± 2.3	5875.749 ± 0.028	81 ± 4
16	sp98	50948.9192	248	3.14	28.8 ± 2.3	5875.732 ± 0.033	77 ± 5
17	sp98	50949.6310	231	2.15	25.7 ± 2.3	5875.802 ± 0.034	69 ± 5
18	sp98	50949.6832	252	2.68	24.1 ± 2.1	5875.796 ± 0.032	67 ± 5
19	sp98	50949.7380	267	2.66	29.6 ± 2.4	5875.780 ± 0.035	85 ± 5
20	sp98	50949.8216	260	2.98	30.2 ± 2.4	5875.751 ± 0.034	83 ± 5
21	sp98	50949.8701	227	3.27	32.8 ± 2.5	5875.673 ± 0.036	84 ± 5
22	sp98	50949.9214	170	2.97	28.5 ± 3.8	5875.697 ± 0.060	85 ± 9
23	sp98	50950.7731	217	2.70	23.9 ± 2.5	5875.656 ± 0.042	71 ± 6
24	sp98	50951.6531	275	2.36	24.9 ± 2.0	5875.608 ± 0.030	70 ± 4
25	sp98	50951.7112	260	2.72	23.7 ± 2.0	5875.695 ± 0.032	67 ± 4
26	sp98	50951.7644	264	2.67	31.0 ± 2.4	5875.755 ± 0.034	85 ± 5
27	sp98	50951.8680	265	3.21	30.6 ± 2.4	5875.615 ± 0.033	83 ± 5
28	sp98	50951.9204	251	2.75	29.9 ± 2.5	5875.655 ± 0.035	83 ± 5
29	fa99	51570.9607	202	3.86	24.4 ± 2.4	5875.801 ± 0.034	62 ± 5

Note.
[a]See Table 1 for observing run information.

Table 9
D_3 Observations for 18 Boo

N	Run[a]	JD–2400000	S/N (pixel^{-1})	RV (km s^{-1})	W_λ (mÅ)	λ_0 (Å)	FWHM (km s^{-1})
1	sp95	49751.0467	124	0.21	37.0 ± 5.0	5875.635 ± 0.043	69 ± 7
2	sp96	50137.0501	80	0.46	30.1 ± 5.8	5875.608 ± 0.065	56 ± 9
3	sp97	50515.0275	126	0.26	23.3 ± 4.3	5875.752 ± 0.051	55 ± 8
4	sp97	50516.0100	66	0.51	41.1 ± 9.9	5875.448 ± 0.083	73 ± 13
5	sp98	50945.6632	167	−0.37	20.2 ± 2.7	5875.784 ± 0.049	59 ± 6
6	sp98	50945.7209	164	0.33	28.4 ± 3.1	5875.553 ± 0.044	70 ± 6
7	sp98	50945.8991	157	0.84	28.3 ± 3.0	5875.675 ± 0.041	65 ± 6
8	sp98	50946.6551	140	−0.38	25.6 ± 3.7	5875.613 ± 0.059	73 ± 8
9	sp98	50946.7134	145	−0.33	21.0 ± 2.7	5875.753 ± 0.038	49 ± 5
10	sp98	50946.7745	147	−0.15	19.1 ± 3.3	5875.691 ± 0.064	66 ± 9
11	sp98	50947.8999	186	0.34	28.8 ± 2.7	5875.643 ± 0.036	67 ± 5
12	sp98	50948.6580	206	0.00	28.1 ± 2.4	5875.700 ± 0.033	67 ± 4
13	sp98	50948.7127	197	−0.06	20.6 ± 2.2	5875.659 ± 0.036	55 ± 5
14	sp98	50948.7653	215	0.25	25.8 ± 2.3	5875.716 ± 0.034	67 ± 5
15	sp98	50948.8388	214	0.43	25.4 ± 2.1	5875.666 ± 0.030	60 ± 4
16	sp98	50948.8933	212	0.65	32.4 ± 2.5	5875.725 ± 0.032	73 ± 4
17	sp98	50948.9453	195	0.23	32.0 ± 2.8	5875.702 ± 0.039	78 ± 5
18	sp98	50949.6572	197	−0.18	19.4 ± 2.2	5875.728 ± 0.036	54 ± 5
19	sp98	50949.7119	217	0.36	20.6 ± 2.1	5875.718 ± 0.035	58 ± 5
20	sp98	50949.7628	213	−0.34	18.0 ± 2.0	5875.647 ± 0.035	52 ± 5
21	sp98	50949.8459	216	0.68	21.3 ± 2.0	5875.641 ± 0.032	56 ± 4
22	sp98	50949.8970	192	0.23	22.5 ± 2.5	5875.669 ± 0.041	64 ± 6
23	sp98	50950.7430	172	−0.59	24.0 ± 2.9	5875.679 ± 0.047	69 ± 6
24	sp98	50950.8026	157	0.25	26.0 ± 3.0	5875.697 ± 0.044	63 ± 6
25	sp98	50951.6818	185	−0.44	15.5 ± 2.1	5875.702 ± 0.036	45 ± 5
26	sp98	50951.7378	202	−0.29	20.1 ± 2.3	5875.659 ± 0.042	60 ± 5
27	sp98	50951.8202	160	−1.22	29.2 ± 3.2	5875.663 ± 0.043	69 ± 5
28	sp98	50951.8956	215	0.23	24.8 ± 2.3	5875.620 ± 0.036	68 ± 5
29	sp98	50951.9453	191	−0.53	20.7 ± 2.2	5875.600 ± 0.035	55 ± 4

Note.
[a]See Table 1 for observing run information.

Table 10
Short-Term Variability Results

Star	Run[a]	$N_{\rm int}$	$\langle W_\lambda \rangle$ (mÅ)	SD[b] (mÅ)	$\langle$Err$\rangle$[c] (mÅ)	$\langle \lambda_0 \rangle$ (Å)	SD[b] (Å)	$\langle$Err$\rangle$[c] (Å)	$\langle$FWHM$\rangle$ (km s^{-1})	SD[b] (km s^{-1})	$\langle$Err$\rangle$[c] (km s^{-1})
ρ Gem	sp97	16	31.5	4.4	3.9	5875.777	0.066	0.052	84.6	10.7	8.2
θ Boo	sp97	7	41.1	1.6	2.5	5875.713	0.037	0.017	54.3	1.8	2.6
θ Boo	sp98	12	33.3	3.2	2.7	5875.701	0.031	0.022	52.3	3.1	3.2
μ Vir	sp98	26	28.5	3.9	2.7	5875.735	0.077	0.040	76.6	7.0	5.8
18 Boo	sp98	25	23.2	4.5	2.6	5875.677	0.048	0.040	61.3	8.2	5.3

Notes.
[a]See Table 1 for observing run information.
[b]Weighted standard deviation of the measurements.
[c]Weighted mean of the measurement uncertainties.

more conservative basis for comparing the standard deviation and measurement uncertainties. Still, a comparison between the standard deviation and typical uncertainties immediately illustrates that we may be seeing significant variability in our sample.

A more formal way to assess variability is to perform a χ^2 test on N measurements of a quantity x with error σ relative to the null-hypothesis of nonvariability using the equation

$$\chi^2 = \sum_i \left(\frac{x_i - \bar{x}}{\sigma_i} \right)^2 \quad (2)$$

and $N - 1$ degrees of freedom (dof). This measures the probability that the sample does not represent a constant variable with normally distributed deviations from the mean, which we call the variability probability. We performed this test not only using the measurement uncertainties reported in Tables 6–9, but also for the possibility that our uncertainties are underestimated by 15%, as discussed in Section 3.7. These results are given in Table 11 and will be discussed on a star-by-star basis.

We can use similar ideas to determine the statistical significance of the difference between two measurements of a value x with error σ, using the Z-statistic:

$$Z = \frac{x_1 - x_2}{\sqrt{\sigma_1^2 + \sigma_2^2}}. \quad (3)$$

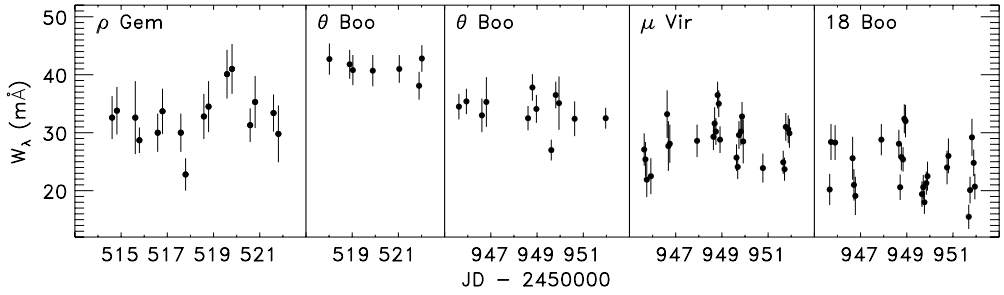

Figure 4. Time series of D_3 equivalent widths.

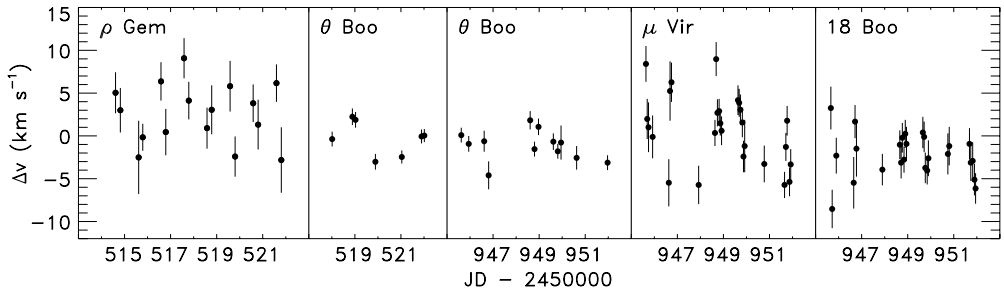

Figure 5. Time series of D_3 line velocities, relative to the sample mean.

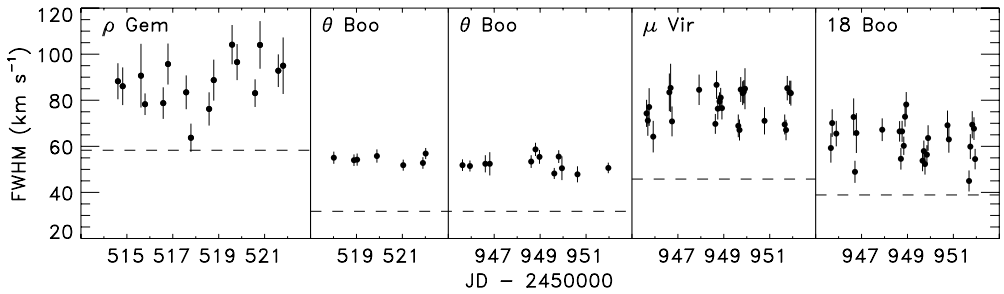

Figure 6. Time series of D_3 linewidths. For comparison, stellar $v \sin i$ is indicated by the dashed lines.

Table 11
Variability Probabilities Using the χ^2 Test

			Reported Errors			15% Greater Errors		
Star	Run[a]	N_{int}	$P_{W\lambda}$	$P_{\lambda 0}$	P_{FWHM}	$P_{W\lambda}$	$P_{\lambda 0}$	P_{FWHM}
ρ Gem	sp97	16	0.922	0.980	0.991	0.716	0.875	0.924
θ Boo	sp97	7	0.140	>0.999	0.183	0.076	0.999	0.101
θ Boo	sp98	12	0.956	0.995	0.696	0.828	0.957	0.443
μ Vir	sp98	26	>0.999	>0.999	0.983	0.987	>0.999	0.838
18 Boo	sp98	25	>0.999	0.960	>0.999	>0.999	0.752	0.998

Note.
[a]See Table 1 for observing run information.

We use this test mostly for long-term variability, but also occasionally in the short-term data set.

In Figures 4–6, we show the time series for the equivalent width, central wavelength, and linewidth for each of the four stars. For convenience, we have expressed the central wavelengths as a velocity relative to the average D_3 wavelength in the sample, 5875.72 Å, consistent with the expected central wavelength of the multiplet. This will make it easier to assess whether any apparent wavelength shifts are a large fraction of the rotational velocity of the stars.

Before discussing each star, we note that since there are several telluric lines within the D_3 profiles, if our removal process does not work well we might see a dependence of the equivalent width on the strength of telluric absorption during that particular exposure. Figure 7 shows these data for each star. The "telluric line depth" corresponds to the strongest line in the vicinity of the sodium D lines, which is much stronger than the lines that interfere with D_3. Clearly, we see no statistically significant trend of D_3 line strength with telluric line strength.

In the following sections, we discuss the four stars from least to most evidence of short-term variability in the D_3 line strength.

5.2. ρ Gem

This star falls well within the usual temperature and spectral class range for early F-type stars and lies at the bottom of the *Hipparcos* main sequence in Figure 3. It has an M-type companion, which is 8 mag fainter visually (Woolley 1970), so it does not contribute light to our spectra. Nordström et al. (2004) reported large radial velocity variability with a standard deviation of 15.0 km s^{-1} based on three measurements covering 3.1 years. Our data cover a 5.0-year period and show at most slight evidence of low-level long-term variability relative to the ∼0.5 km s^{-1} uncertainties, and our velocities are similar to others referenced by SIMBAD.

We observed the star twice per night during each of the eight nights of the sp97 run. In this data set, the equivalent width, central wavelength, and linewidth show weighted standard

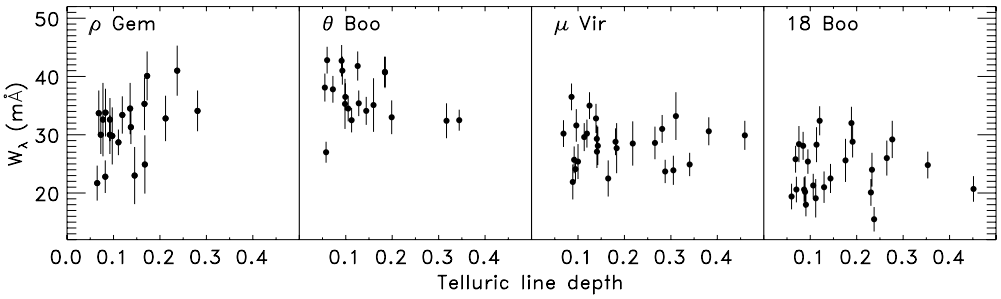

Figure 7. D_3 equivalent width vs. telluric line strength. The latter is based on the strongest telluric line in our fit range.

deviations that are about 10%–25% greater than the mean uncertainties of the original values. Thus, as Table 6 indicates, a claim of variability requires that our uncertainties are accurately specified.

The time series in Figure 4 shows that there is one observation with a small equivalent width (number 10 in Table 6) and that both observations from the sixth night (numbers 13 and 14 in Table 6) are relatively high. These three points provide almost exactly half of the total χ^2, and even with our reported measurement uncertainties, the χ^2 probability is not at a level where we would claim variability.

The variability probabilities are greater for both central wavelength and FWHM. The central wavelength does not show a particular pattern, but rather a scatter that appears larger than the uncertainties while remaining a small fraction of v sin i. The FWHM mostly follows the pattern seen for the equivalent width, but with larger differences between the two nightly measurements for several nights.

Overall, we do not find strong evidence of variability in the strength of the D_3 line in ρ Gem. The evidence is slightly stronger for the central wavelength and linewidth, but requires that our measurement uncertainties are not underestimated.

5.3. θ Boo

This is clearly a late F-type star that falls under the category of "solar-type," that is, it is on the cool side of the point near spectral type F5 where stars begin to show activity levels related to the strength of the magnetic dynamo via rotational speed and age (e.g., Simon & Drake 1989; Wolff & Simon 1997). As Figure 2 shows, this star appears to be about twice as luminous as a zero-age main-sequence star of the same color; thus, it is either near the end of its main-sequence lifetime or is a binary system with nearly equal components. We see some evidence of radial velocity variations in our data, and Nordström et al. (2004) indicated both radial velocity variability and an advanced age for this star (3.1 Gyr). However, we did not detect spectral lines from a secondary star, and presume that any companion is faint. Another possibility is that the two stars show minimal velocity separation due to their orbit, for example, a small inclination. In that case, the two stars would have to have very similar spectral types, abundances, and rotational velocities. Speckle interferometry by McAlister et al. (1992) constrains any companion to a separation of less than 0.″03 and Δm greater than 1.5 mag. For our purposes, this star was chosen due to small v sin i, strong D_3 line, and its brightness, which gave us the most precise data of the four stars with integration times of 20 minutes.

We obtained repeated observations of this star in two different observing runs. In the sp97 run, we obtained seven spectra over the course of five consecutive observing nights, while in the sp98 run, we obtained 12 spectra across six of the seven nights. Figures 4–6 show both of these time series.

We only see limited evidence of variability in the equivalent width or FWHM in both runs. The χ^2 value and resulting probability for equivalent width variability in the sp98 run are fairly large, but most of the total χ^2 is due to a single point, number 17 in Table 7. Still, we see nothing unusual about the spectrum or the fit that would invalidate this point. If we compare this value with that from the 18th exposure taken 4.6 hr later, the Z-statistic gives a 3.3σ difference, corresponding to only a 0.1% probability that these two values result from a purely statistical variation.

The χ^2 values indicate strong support for variability in the central wavelengths, particularly in the sp97 run. Figure 5 clearly shows the putative variation, which covers a range of about 5 km s^{-1} as compared with v sin $i = 31.8$ km s^{-1}. As noted in Table 5, we calculate a maximum possible rotational period (P/sin$i$) of 2.8 days for this star. Thus, the combination of a statistically constant D_3 equivalent width with an apparent oscillation in the central wavelength over a few days would be consistent with rotational modulation of one or more strong active longitudes analogous to the Sun. The low amplitude of the velocity variation in the line would imply that the overall activity was broadly distributed across the disk. While this is a plausible hypothesis, the data from the sp98 run do not as clearly show this pattern, although the central wavelength does appear to be variable.

5.4. μ Vir

As noted in Section 1, there is some evidence in the literature of chromospheric variability. As seen in Figure 3, this star is located at the top of the *Hipparcos* main sequence, consistent with being slightly evolved, although our derived surface gravity is similar to main-sequence stars. It is also the brightest star of the short-term variability sample and thus we were able to obtain 26 observations during the eight nights of the sp98 run with typical integration times of 15 minutes. As with ρ Gem, Nordström et al. (2004) reported significant radial velocity variability with a standard deviation of 12.4 km s^{-1} in three measurements covering 1.4 years. Abt & Levy (1976) reported a possible variability of about 10 km s^{-1} in 21 measurements spread over 4.8 years with a possible period of 0.9 years. However, our measurements over 4.1 years (with intervals among observations of 1.2, 1.3, and 1.7 years) only support the possibility of a years-scale variation of up to 2 km s^{-1}, a much smaller range than either previous data set.

The χ^2 analysis provides strong evidence of equivalent width variability in our sample. This variation is most easily seen in Figure 4 by comparing the first and fourth night's worth of data. Interestingly, the appearance in the time series is that of a gradual rise in activity over the first four nights, followed by a decrease. However, the value of the maximum possible rotational period (P/sin$i$) in Table 5 is just 2.2 days. Thus, this trend represents a more gradual variation than would be explained by rotation. In addition to night-to-night variability, the time series also indicates variability within a single night, particularly on the final night. We do not find significant periodicities at either timescale with a periodogram analysis.

The variability probabilities for central wavelength are extremely close to 1. This variability is evident in the time series in Figure 5 and appears strongest on short timescales within a night. The total range of the line centers is 15 km s^{-1}, which is still a relatively small fraction of the D_3 line width or v sin i. A key point is that the variability occurs on a much shorter timescale than rotation.

In a statistical sense, the variability in the wavelength is more pronounced than that for the equivalent width. One possibility is that if the activity is spread across the disk in some way, a rapid redistribution in point-to-point activity levels could affect the disk-averaged central wavelength without affecting the equivalent width as much. One test of this hypothesis would be to look for subtle line asymmetries, but at the S/N of our data we cannot confirm this possibility.

5.5. 18 Boo

As already noted, the literature values for the D_3 equivalent width significantly disagree. The star lies near the bottom of the *Hipparcos* main sequence in Figure 3, and it is a possible member of the Ursa Major Moving Group (Soderblom & Mayer 1993; King et al. 2003), which would also imply a relatively young age of 300–500 Myr. Our radial velocities in Table 9 show no evidence of variability nor did we locate other evidence to support classification as a spectroscopic binary although it is a wide visual binary.

This star shows very strong evidence of line strength variability, the strongest in the present sample. Figure 4 clearly shows the variability, and the probabilities in Table 11 are very large. The variability on the fourth and seventh nights is highly pronounced and covers a large fraction of the range seen in the full sample. In contrast, the line strength is tightly clustered on the fifth night. It is important to note that the observed variability in 18 Boo on the fourth and seventh nights is not matched by μ Vir on those nights. For all spectra of the two stars, if one star was observed the other star was observed immediately before and/or after. This gives further support to the hypothesis that our observed variability is not a data analysis artifact. As with μ Vir, we do not find strong evidence of periodicities in the time series.

To further illustrate the line variability, we show a stack plot of all 25 spectra from the sp98 run in Figure 8, along with the Gaussian fits. The variability can be most clearly seen near the top, as well as when looking closely at the variable spacing between adjacent spectra at the line core, despite the uniform spacing of the continua.

The variability probabilities for the linewidths are similar to those for line strength. A comparison of Figures 4 and 6 indicate that the putative variability in both quantities is related and this relationship between the equivalent width and FWHM

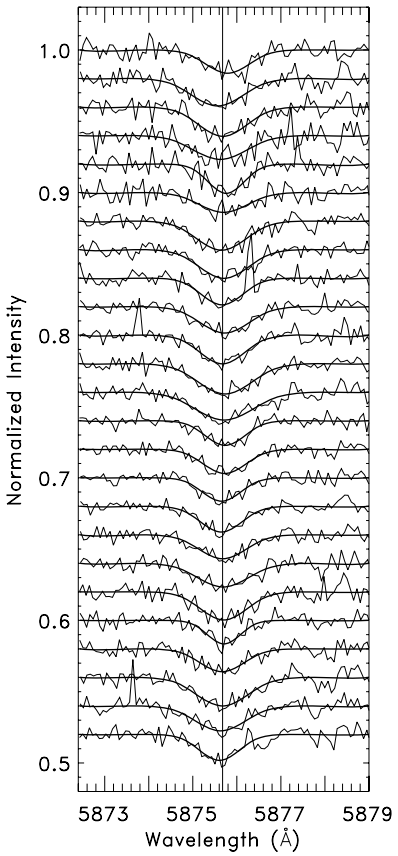

Figure 8. D_3 spectra and fits for 18 Boo for the sp98 data set. All 25 spectra are shown in a chronological order from top to bottom. The occasional upward spikes in the data are due to radiation events in the CCD and carry negligible statistical weights in the line fits. Significant variations are visible, especially near the top.

is most pronounced for 18 Boo. The variability probabilities are smaller for the central wavelength. The total velocity range of about 12 km s^{-1} is covered by the spectra on the first night, with a smaller range for the rest of the data. As with μ Vir, the implication is that the variability operates on nonrotational timescales.

Based on our measurements, we believe that the large difference in the two previous literature values of equivalent width represents the same variability that we have observed. Indeed, these measurements provide a good match to the high and low values of the equivalent width that we report.

As one final additional test of our D_3 results, we fitted several photospheric lines to see if these lines appeared variable. Since 18 Boo shows the strongest evidence of D_3 variability, we give those results in Table 12, which are also representative of μ Vir. We se that for two lines that are somewhat stronger than D_3 and one line that is comparable to the weakest D_3 measurement, the standard deviation of the line measurements is nearly identical to the measurement uncertainties. A χ^2 analysis gives variability probabilities generally in the range 0.4–0.8, supporting the idea that our measurement techniques do not create the appearance of variability in the D_3 lines where none is present. Out of the nine probabilities, only one is greater than 0.9, but that is for the central wavelength of the weakest line, and only a few of our D_3 lines in 18 Boo are that weak. Furthermore, a Gaussian is not as good of a match to the photospheric lines as for the D_3 line and that might contribute to larger fluctuations in the fits.

Table 12
Photospheric Line Fits for 18 Boo During sp98

Line	N_{int}	$\langle W_\lambda \rangle$ (mÅ)	SD[a] (mÅ)	$\langle$Err$\rangle$[b] (mÅ)	$\langle \lambda_0 \rangle$ (Å)	SD[a] (Å)	$\langle$Err$\rangle$[b] (Å)	$\langle$FWHM$\rangle$ (km s^{-1})	SD[a] (km s^{-1})	$\langle$Err$\rangle$[b] (km s^{-1})
Fe I λ5816	25	55.2	3.5	3.6	5816.375	0.014	0.016	54.2	2.6	2.8
Fe I λ5848	25	16.5	2.4	2.2	5848.090	0.043	0.038	54.1	5.9	5.8
Fe I λ5934	25	52.1	2.6	3.0	5934.636	0.017	0.017	55.3	2.3	2.6

Notes.
[a]Weighted standard deviation of the measurements.
[b]Weighted mean of the measurement uncertainties.

Table 13
Additional D_3 Observations

Star	Run[a]	JD–2400000	S/N (pixel^{-1})	RV (km s^{-1})	W_λ (mÅ)	λ_0 (Å)	FWHM (km s^{-1})
β Cas	fa95	50052.5386	205	5.94	21.8 ± 4.5	5875.381 ± 0.138	142 ± 22
β Cas	sp98	50948.9820	219	10.40	23.9 ± 3.9	5875.408 ± 0.132	154 ± 20
β Cas	fa99	51570.5511	311	7.75	14.8 ± 2.2	5875.453 ± 0.100	119 ± 14
9 Aur	sp96	50136.5929	67	−1.57	15.6 ± 6.2	5875.996 ± 0.112	47 ± 15
9 Aur	sp97	50521.6403	152	−2.58	20.3 ± 2.7	5875.823 ± 0.040	50 ± 5
η Lep	fa95	50057.7213	165	−0.78	35.6 ± 2.7	5875.699 ± 0.020	47 ± 2
η Lep	fa96	50373.9985	215	−0.91	31.2 ± 2.1	5875.778 ± 0.018	51 ± 2
η Lep	sp97	50520.5941	199	−0.86	32.6 ± 2.2	5875.746 ± 0.022	53 ± 3
α CMi	sp96	50137.5669	183	−3.00	6.5 ± 2.5	5875.693 ± 0.129	56 ± 17
α CMi	sp96	50142.7192	281	−2.78	8.8 ± 1.6	5875.451 ± 0.061	56 ± 8
α CMi	sp97	50521.6544	314	−2.31	7.0 ± 1.5	5875.707 ± 0.069	57 ± 9
χ Leo	sp95	49754.0362	263	4.51	3.7 ± 1.2	5875.556 ± 0.060	31 ± 8
χ Leo	fa96	50374.0236	245	5.80	6.3 ± 1.9	5875.602 ± 0.108	63 ± 15
χ Leo	sp97	50520.9079	214	6.58	4.7 ± 2.0	5875.587 ± 0.106	42 ± 15
χ Leo	sp98	50951.6350	162	6.40	...	...	...
χ Leo	fa99	51565.0614	158	6.05	4.5 ± 1.9	5875.577 ± 0.068	27 ± 9
α Crv	sp95	49754.0651	226	3.00	21.5 ± 1.8	5875.749 ± 0.024	50 ± 3
α Crv	sp97	50517.8913	187	4.87	26.3 ± 2.5	5875.760 ± 0.037	65 ± 5
σ Boo	fa95	50052.0561	187	1.66	7.3 ± 1.6	5875.695 ± 0.040	29 ± 5
σ Boo	sp97	50521.9554	145	1.05	13.7 ± 2.1	5875.640 ± 0.028	29 ± 3
μ^1 Boo	fa95	50056.0338	167	−9.08	17.5 ± 3.8	5875.567 ± 0.075	74 ± 13
μ^1 Boo	sp97	50519.0146	177	−7.09	24.1 ± 7.0	5875.610 ± 0.107	115 ± 24
μ^1 Boo	sp98	50951.8521	91	−1.83	...	...	...
σ Ser	sp95	49752.0628	189	−49.33	35.0 ± 4.5	5875.966 ± 0.057	107 ± 10
σ Ser	sp97	50521.9777	181	−50.77	28.0 ± 4.1	5875.891 ± 0.064	95 ± 11
HR 6237	fa95	50050.5463	152	−18.96	23.1 ± 2.9	5875.873 ± 0.047	61 ± 6
HR 6237	sp97	50521.9927	173	0.64	23.6 ± 2.9	5875.740 ± 0.040	60 ± 6
ξ Oph	sp96	50143.0288	113	−9.51	19.4 ± 3.1	5875.762 ± 0.039	39 ± 5
ξ Oph	sp97	50522.0047	153	−8.25	21.9 ± 2.5	5875.745 ± 0.032	47 ± 4

Note.
[a]See Table 1 for observing run information.

6. LONG-TERM VARIABILITY

6.1. Preliminary Comments

We obtained additional measurements of the four stars in the short-term sample to look for long-term variability, and these measurements have already been presented in Tables 6–9. Table 13 provides measurements of an additional 11 stars for which we obtained measurements in at least two different observing runs and we give the same data as for the short-term sample. In the rest of this section, we make note of the literature values of the D_3 equivalent width where available. While one cannot exactly compare these results due to differences in the telluric and photospheric line removal procedures, those values should at least be similar to ours if there is no variability. As with the short-term study, we give heliocentric radial velocities. Again, we want to make sure that the D_3 lines are not being "polluted" by a cooler star or that binarity affects the activity levels. In no case did we see any spectral lines from a secondary component.

6.2. Long-term Variability in the Short-term Sample

As seen in Tables 6–9, for all four stars in the short-term sample we obtained spectra in at least three additional observing runs. These values are broadly consistent with the short-term variability (or lack thereof) seen in the large samples within a single observing run.

The evidence of equivalent width variability for both ρ Gem and θ Boo becomes more significant when including the additional data. For ρ Gem, three out of the four additional spectra (numbers 1, 2, and 20 in Table 6) show equivalent widths considerably smaller than the bulk of the sp97 sample. In fact, these values match the single low point (number 10) seen in that sample. If we include all 20 measurements of ρ Gem, the

probability of the equivalent width variability rises to 0.994 with our reported uncertainties and 0.926 if our uncertainties are underestimated by 15%.

Our two sets of observations for θ Boo indicate long-term variability. If we compare the values in Table 10, 41.1 ± 1.6 mÅ for sp97 and 33.3 ± 3.2 mÅ for sp98, we derive a 2.2σ difference using the *Z*-statistic, and this does not take into account a $\sqrt{N}$ reduction in the uncertainty if we used the sample standard deviation. Notably, all seven equivalent widths from sp97 are larger than all 12 values from sp98.

Previous investigators have reported equivalent widths for all four stars. We have already mentioned that the previously discrepant 18 Boo measurements are consistent with our observed variability. Previous values for ρ Gem match the high end of our measurements; 38 mÅ from Wolff et al. (1986) and seven measurements of 30.0–48.2 mÅ from Teresova (2005). Wolff et al. (1986) found an average equivalent width for μ Vir of 19 mÅ from 12 measurements, somewhat smaller than our average of 28.5 mÅ. Finally, Wolff et al. (1986) found an equivalent width of 35 mÅ for θ Boo and Teresova (2005) found 27.7–36.2 mÅ in five measurements; these values are generally consistent with ours.

6.3. Additional Stars in the Long-term Sample

6.3.1. β Cas

This star lies well above the main sequence in the Hertzsprung Gap, and has by far the smallest surface gravity in our sample. The star has one of the largest $v \sin i$ values in the sample, and thus the radial velocities are particularly uncertain and not indicative of variability. We have already mentioned the possible UV emission line variability in Section 1.

As found by Rachford (1997), giant stars in this temperature range show similar D_3 equivalent widths as dwarfs, and our D_3 equivalent widths for β Cas are typical for early F-type stars. The first two equivalent widths are statistically identical, but the third value differs from the second value at the 2.0σ level.

Interestingly, while the central wavelengths of the D_3 line are not statistically variable, they consistently deviate to the blue. An average of the three measurements yields 5875.41 ± 0.15 Å, or a blueshift of 16 ± 7 km s^{-1} relative to the 5875.72 Å mean found for the short-term sample. Ayres et al. (1998) found similar blueshifts for the O IV 1401, C IV 1548, and C IV 1550 lines and similar amounts of excess broadening beyond the photospheric $v \sin i$. These lines form at temperatures near 10^5 K, while the D_3 line is thought to form at temperatures near 10^4 K. However, other UV emission lines that form at temperatures comparable to D_3 did not show these blueshifts.

6.3.2. 9 Aur

This star is one of the best-studied γ Doradus nonradial pulsating variables (Krisciunas 1995). There is a 12th magnitude M-type component 5 arcsec from the main star, which is too faint to affect our spectra. Our first D_3 measurement is rather uncertain, but no variability is detected.

6.3.3. η Lep

This star lies very near 9 Aur on the *Hipparcos* color–magnitude diagram in Figure 3 with similar temperature and gravity, but appears not to show significant photometric or radial velocity variability. In particular, Nordström et al. (2004) reported statistically constant radial velocity in 13 measurements covering 16.3 years, and our three measurements spanning 1.3 years agree with this conclusion.

The equivalent widths and line widths for the three observations are statistically identical. However, the central wavelength for the first and second observations disagree at the 2.9σ level based on the *Z*-statistic. The wavelength difference corresponds to a velocity difference of 3.9 ± 1.2 km s^{-1}, a small fraction of $v \sin i = 17.4$ km s^{-1}. This implies a situation similar to that for μ Vir where there may be some sort of redistribution of activity that causes little if any equivalent width variability, but slightly distorts the shape of the line leading to a change in the measured line center.

6.3.4. α CMi (Procyon)

Procyon was observed not only because it is the brightest main-sequence F-type star, but also because at spectral type F5 and $B-V = 0.42$ it is at the high temperature edge of solar-type stars, which show activity–rotation–age correlations (e.g., Simon & Drake 1989; Wolff & Simon 1997). This star exhibits low-amplitude variability in the Ca II H & K lines (Baliunas et al. 1995). Danks & Lambert (1985) found a D_3 equivalent width of 5 mÅ and our three values are similar and highly consistent, as are the line widths.

In contrast, the central wavelength of the second observation is considerably bluer than the other two measurements. The *Z*-statistic indicates that the second and third measurements differ at the 2.8σ level. Given that this appears to be a solar-type star, the situation may be similar to what we found for θ Boo, a variation in the wavelength due to the rotational modulation of active regions. It is important to note that the first two observations were made just 5 days apart and $P/\sin i$ for Procyon is 18.5 days; thus, our observations likely cover something close to one-quarter of a full rotation. The wavelength difference between these two observations corresponds to 12 ± 7 km s^{-1}. Recall that we found $v \sin i = 5.3$ km s^{-1}, which would also be the maximum observable velocity range for one-quarter of a period. Allende Prieto et al. (2002) derived $v \sin i = 3.2$ km s^{-1} from a more sophisticated three-dimensional model atmosphere. Thus, our results are statistically consistent with rotational modulation, with the caveat that our first measurement is rather uncertain.

6.3.5. χ Leo

This star is an interesting case due to the very weak D_3 line for an otherwise normal, but slightly evolved early F-type star. We see evidence of long-term radial velocity variability, but this mostly appears in the sp95 observation for which there may be a slight zero-point offset relative to other runs due to the more limited wavelength coverage. We did not find significant evidence of radial velocity variability in the literature.

For the four spectra in which we could measure the D_3 line at the 2σ level or greater, the measurements are statistically identical. We were unable to obtain a statistically significant D_3 detection in the sp98 data, but given the weakness of the line in the other spectra, this nondetection is consistent with the other measurements.

Although somewhat uncertain, the linewidths are relatively narrow. The weighted mean and weighted standard deviation for the four D_3 detections give FWHM $= 35 \pm 13$ km s^{-1}, as compared with $v \sin i = 27.5$ km s^{-1}. Although σ Boo (see below) has a very narrow D_3 line, it also has very small $v \sin i$, and χ Leo is the only star in our present sample with an average D_3 linewidth only slightly broader than photospheric lines. For

comparison, α CMi also shows a consistently weak D_3 line, but with FWHM = 56–57 km s^{-1}, indicating the effects of greater thermal and turbulent broadening for D_3 as compared with photospheric lines.

In principle, a small equivalent width for a D_3 line in an F-type star suggests a low active-region filling factor (Andretta & Giampapa 1995), although the hottest star considered in that study was 6500 K. In turn, a small active-region filling factor would generally produce a narrower line than the case of a larger filling factor, particularly if the activity were constrained to a limited longitude range and/or high latitudes. Rachford (2000) found one other case of an unusually narrow D_3 line in a Pleiades star (H II 1266), but in that case the D_3 line was clearly narrower than v sin i even when not compensating for the larger thermal and turbulent broadening for D_3. Activity concentrated at high latitudes was invoked to explain the contradiction in linewidths. In that case, v sin i = 76.6 km s^{-1}, so it was much easier to rule out spectrum-to-spectrum wavelength shifts in the D_3 line to within very small fraction of rotational broadening and thus mostly rule out rotational modulation of an active region at a single stellar longitude. Since χ Leo has one-third as much rotational broadening as the Pleiades star, our wavelength uncertainties amount to 10%–20% of v sin i. Thus, even though our D_3 central wavelengths show no variability within the precision of our measurements, we cannot as easily rule out rotational modulation.

6.3.6. α Crv

This star lies at the bottom of the *Hipparcos* main sequence, although the spectral classification indicates a slightly evolved star. The heliocentric radial velocity difference between our two observations would be statistically significant, but as already mentioned, we have concerns about the zero point of the sp95 observations. Nordström et al. (2004) found a strong likelihood of radial velocity variability in 20 measurements over 14.9 years. We see no significant difference between the two D_3 measurements.

6.3.7. σ Boo

This star lies at the bottom of the *Hipparcos* main sequence. Nidever et al. (2002) found radial velocity scatter less than 0.1 km s^{-1} based on high-precision observations used in a search for exoplanets. Note that our velocities are about 1 km s^{-1} greater than theirs, which gives some indication of the systematic errors that may exist in our radial velocity measurements.

The two D_3 equivalent widths differ by 2.4σ via the Z-statistic. The literature values are consistent with the possibility of variability as Wolff et al. (1986) found an equivalent width of 8 mÅ, while Teresova (2005) found 19.0 mÅ. Our central wavelength and linewidth measurements are not statistically different.

6.3.8. μ^1 Boo

This star has the largest v sin i in our sample. It has a wide companion nearly 2 arcmin away which is itself a long-period binary (μ^2 Boo). Photographic spectra indicate at best low-amplitude radial velocity variability (Niehaus et al. 1970; Abt & Levy 1974). Our data are also of relatively low precision due to the large v sin i and low S/N for the observation that appears to differ from the other two.

The two observations in which we detect D_3 show reasonable statistical agreement. We do not conclusively detect D_3 in the low-quality observation. However, depending on the width of a putative D_3 line, the 2σ upper limit could be comparable to the other observations.

6.3.9. σ Ser

Our D_3 measurements are statistically identical and given the relatively large v sin i and the possible zero-point issue with the sp95 data, the heliocentric radial velocities are likely nonvariable. Wolff et al. (1986) found an equivalent width of 23 mÅ and Teresova (2005) found 29.2 mÅ, broadly consistent with our values.

6.3.10. HR 6237

This star is a single-line spectroscopic binary with a period of 3.8 years (Abt & Levy 1974). Our two radial velocity measurements are broadly comparable to those results. The wavelength of the D_3 line differs by 2.2σ between the two observations, but the line strength and width are nearly identical.

6.3.11. ξ Oph

This star is a visual binary with Δm = 4.0 and a separation of 14.4 arcsec. Our radial velocities suggest variability, as do the three observations by Nordström et al. (2004) covering 263 days. However, the D_3 measurements are nearly identical in all three parameters.

7. DISCUSSION

Our results for 18 Boo and to a lesser extent μ Vir appear to establish the reality of short-term chromospheric variability in some fraction of early F-type stars. Both stars appear to be single with no reported optical variability in *Hipparcos* observations or other literature sources. Stellar parameters are quite similar for the two stars, although μ Vir appears to be somewhat evolved toward the terminal-age main sequence while 18 Boo appears to be very near the zero-age main sequence, consistent with its possible membership in the Ursa Major Moving Group.

The physical nature of this variability is not clear, but we can explore various situations involving rotation. While we do not know the sin i factors for individual stars, the maximum possible value of v should be similar to or less than the largest v sin i seen in young clusters. For the Pleiades and Alpha Persei clusters, Kraft (1967) found early F-type stars with v sin $i \sim$ 200 km s^{-1}. Even in that extreme case, the rotational period would still be $\sim$8 hr and pure rotational modulation of isolated active regions would not seem to be responsible for the variability we see. Furthermore, even in the early F-type stars, rotation slows down with age and with decreasing effective temperature. In fact, for the temperature range of our field stars, $\langle v \sin i \rangle$ is about 30–50 km s^{-1} (Wolff & Simon 1997). Thus, the three early F-type stars in the short-term sample have nearly average values of v sin i and are not likely to be viewed nearly pole-on. Thus, the rotational periods will be much closer to the values in Table 5 than they are to the hypothetical minimum value of $\sim$8 hr. We have already noted that we do not find any clear periodicities in the equivalent widths, albeit the temporal coverage is limited.

Furthermore, the D_3 line in this temperature range is purely chromospheric, for example, in the Sun the line is only seen in conjunction with plages (Landman 1981). Thus, the line only samples the portions of the rotational broadening function at speeds corresponding to the apparent velocities at those stellar longitudes. If we see rotational modulation of a small number of isolated active regions, we should see velocity shifts (or

asymmetries) in the D_3 line that are a large fraction of v sin i, unless the active regions are all at high latitudes. However, Figure 5 clearly shows that such large shifts are not observed. The total velocity range of the D_3 line for both 18 Boo and μ Vir is less than 20% of the quantity $2 \times v$ sin i. Moreover, the rotational modulation produced by high-latitude features would be less likely to explain the full range of equivalent width variation that is seen for these two stars.

Another aspect of significant axial inclination is that we would mostly be observing polar regions. In the Sun, activity is concentrated near the equator; thus in other stars with sun-like activity, over time we should see activity covering the full range of equatorial rotation. However, the other consequence of observing polar regions is the possibility of significant stellar oblateness. Interferometric studies of rapidly rotating ($\sim$200 km s^{-1}) A-type stars indicate that such stars can be highly oblate, which causes the surface temperature to be considerably hotter in the polar regions (e.g., van Belle et al. 2001). Thus, a star may be cool enough at the equator for convective activity while being hot enough near the poles to shut off convection. This effect could influence the observed strength and distribution of active regions on the star and thus the appearance of chromospheric spectral features (e.g., Freire Ferrero et al. 1995). However, we have no evidence that the stars in our sample rotate at such high speeds. Plus, this effect would merely mimic the observed situation on the Sun where activity tends to lie near the equator.

Our results suggest that the observed variability must result from either some sort of a global phenomenon or significant variations of a large number of small active regions. Either of these possibilities could produce significant short-term activity variations without large velocity variations or obvious periodicity, and thus no observable relationship with rotation.

As a final note on short-term variability, it is worth considering in more detail the actual distribution of equivalent width values in our sample. We have already shown with the χ^2 analysis that the equivalent widths for both 18 Boo and μ Vir significantly differ from a Gaussian distribution of width comparable to the measurement uncertainties. In Figure 9, we give histograms of the equivalent widths for both stars. If changes in activity were mostly the result of some level of flaring on the top of a basal level of activity, we might expect many points for a star to be clustered in the low end of the distribution with a noticeable "tail" of larger equivalent widths. If the activity were somehow related to a "high/low state" phenomenon, we would expect a bimodal distribution (a similar result would occur if we were seeing a purely sinusoidal variation whereby the star would spend more time near the peak and trough of the variation). However, we see nothing conclusive in the distributions. For both stars the distributions look like something in between a broad Gaussian and a uniform distribution, with just a couple of high points for 18 Boo. Admittedly, with our limited number of data points, the $\sqrt{N}$ errors are large in the histograms, but the point is that we do not see a clear pattern that would indicate a well-defined mode of variability.

As for the long-term variations, we can only claim 2σ variability in the D_3 equivalent width for two of the 11 stars in the purely long-term sample, β Cas and σ Boo. Given the apparent short-term variability we have found in μ Vir and 18 Boo, it may be difficult to claim long-term variability based on a small number of measurements because a significant difference between two measurements widely separated in time might simply be due to the short-term variability.

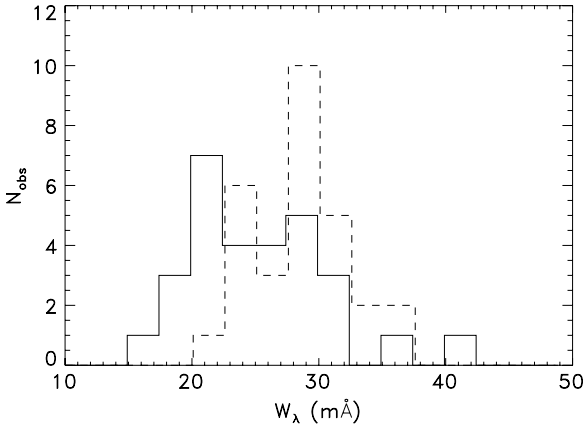

Figure 9. Histograms of D_3 equivalent widths. The solid line corresponds to 18 Boo and dashed line corresponds to μ Vir. The binsize of 2.5 mÅ was chosen as an approximate match to the typical measurement uncertainties, and the two histograms are slightly offset horizontally for clarity.

However, we can use the short-term results to set an expectation on how often we might find such variability in the long-term sample, even if there is no true long-term variability. We can take all combinations of the short-term observations for a star and see how often we get a Z-statistic greater than 2.0 or 3.0. For ρ Gem, there are 120 possible pairs of observations that can be chosen, 14 (11.7%) of which have $Z > 2.0$, including just two (1.7%) with $Z > 3.0$. In contrast, for 18 Boo there are 300 possible pairs of observations, 88 (29.3%) of which have $Z > 2.0$, including 29 (9.7%) with $Z > 3.0$. Naturally, we can also note that if all stars are constant, we expect only 4.6% of a large sample to show $Z > 2.0$ and 0.3% with $Z > 3.0$.

Our finding of only two out of 11 stars with possible long-term variability is thus most consistent with the minimal or nonexistent short-term variability of ρ Gem. However, given the small sample size, this finding is also consistent with the other two possibilities. The key is that our results do not suggest significant excess long-term variability in the early F-type stars beyond variability which can be explained by short-term effects, unless the long-term variability happens on very long timescales. If long-term variability were important on several year timescales, we might expect a large fraction of our long-term sample to show variations due to a combination of short-term and long-term variability and that appears not to be the case.

However, we do not have enough information to support an explanation for why we do not see variability in more stars. Given the long-term data for ρ Gem, the combination of bad luck and slightly poorer data quality may have conspired to hide more obvious short-term variability. In fact, we certainly cannot rule out the possibility that all early F-type stars exhibit variability at a level that would be detected by a large number of observations at a precision comparable to our best data. It is worth noting that most stars in the long-term sample have average line strengths below that of the short-term sample, making it more difficult to detect activity variations at a given fractional level.

As far as the activity levels themselves are concerned, it is clear from a variety of studies using numerous activity indicators that the early F-type stars exhibit a wide range in activity, even when considering a narrow temperature range. This is true for chromospheric emission lines such as C II λ1335 (Simon & Landsman 1991) and Lyman α (Landsman & Simon 1993), and X-ray emission (Schmitt et al. 1985). Results for the D_3

line are similar (García López et al. 1993; Rachford 1997, 2000). However, the results of these studies can rule out some mechanisms that might explain the range, such as the luminosity class (Rachford 1997), age (Rachford 2000), and rotational velocity (Simon & Landsman 1991; Rachford 1997).

An important motivation for the present study was to assess whether short-term and/or long-term variability can explain the large range in activity levels. This does not appear to be the case. Among the most persuasive arguments to support this conclusion are the general lack of significant variability in the long-term sample and the fact that χ Leo seems to have consistently very low activity. Stars such as σ Ser and η Lep are near χ Leo on the color–magnitude diagram and have very similar temperatures and gravities, but have D_3 line strengths a factor of $\sim$5 greater. Thus, if variability is responsible for this difference, it must happen on timescales longer than a few years. Furthermore, the general agreement we see between our measurements and those reported by other authors many years before and/or after also suggests that long-term variability is not a major factor.

8. CONCLUSIONS

We have performed the most detailed study to date on chromospheric variability in the early F-type stars. Through a combination of intensive observations of four stars over intervals of several days and occasional observations over a period of a few years for these stars plus an additional 11 stars, we have searched for variations in the strength, wavelength, and width of the helium D_3 line. The key aspects of our study are the rigorous procedures used to eliminate contaminating telluric and photospheric lines from the chromospheric D_3 line and our careful assessment of measurement uncertainties.

We find significant evidence of short-term (hours to days) variability in two early F-type stars, amounting to about a factor of 2 in equivalent width. The central wavelength of the line also shows evidence of variability, but this variability covers a small fraction of the total range due to rotational broadening. Our data do not support a simple explanation associated with pure rotational modulation of discrete active regions or active longitudes for the early F-type stars, but this explanation does appear to apply to the short-term variations seen in the two coolest stars, α CMi and θ Boo.

In a statistical sense, the small number of stars in the long-term sample showing possible variability is consistent with the idea that some small fraction of early F-type stars show short-term variability large enough to be detected at our measurement precision. However, the long-term sample does not point to the likelihood of variability on the scale of years in the early F-type stars beyond that, which can be explained by short-term variability.

Finally, the general lack of variability larger than a factor of 2 implies that variability is not an explanation for the large range in activity levels seen in the early F-type stars, and this range remains unexplained.

We thank the referee for very helpful comments on the manuscript. We would also like to thank D. Smith for his careful reading of the manuscript and A. Gretarsson for discussions concerning statistical analysis. This research has made use of the SIMBAD database, operated at CDS, Strasbourg, France. Participation by D.R.F. was supported by a NASA traineeship grant provided by the Arizona/NASA Space Grant Consortium.

REFERENCES

Abt, H. A., & Levy, S. G. 1974, ApJ, 188, 291
Abt, H. A., & Levy, S. G. 1976, ApJS, 30, 273
Allende Prieto, C., Asplund, M., García López, R. J., & Lambert, R. J. 2002, A&A, 567, 544
Andretta, V., & Giampapa, M. 1995, ApJ, 439, 405
Ayres, T. R. 1991, ApJ, 375, 704
Ayers, T. R. 1999, ApJ, 525, 240
Ayres, T. R., Simon, T., Stern, R. A., Drake, S. A., Wood, B. E., & Brown, A. 1998, ApJ, 496, 428
Balachandran, S. 1990, ApJ, 354, 310
Baliunas, S. L., et al. 1983, ApJ, 275, 752
Baliunas, S. L., et al. 1995, ApJ, 438, 269
Barnes, T. G., & Evans, D. S. 1976, MNRAS, 174, 489
Bevington, P. R., & Robinson, K. R. 1992, Data Reduction and Error Analysis for the Physical Sciences, (2nd ed.; New York: McGraw-Hill)
Biazzo, K., Frasca, A., Henry, G. W., Catalano, S., & Marilli, E. 2007, ApJ, 656, 474
Boesgaard, A., Budge, K. G., & Burck, E. E. 1988, ApJ, 325, 749
Burkhart, C., & Coupry, M.-F. 1991, A&A, 249, 205
Cayrel de Strobel, G., Soubiran, C., Friel, E. D., Ralite, N., & Francois, P. 1997, A&AS, 124, 299
Danks, A. C., & Lambert, D. L. 1985, A&A, 148, 293
Edvardsson, B., Andersen, J., Gustafsson, B., Lambert, D. L., Nissen, P. E., & Tomkin, J. 1993, A&A, 275, 101
Edvardsson, B., Gustafsson, B., & Nissen, P. E. 1984, Messenger, 38, 33
ESA 1997, The Hipparcos and Tycho Catalogues, (ESA SP-1200; Noordwijk: ESA)
Fekel, F. C. 1997, PASP, 109, 514
Frasca, A., Freire Ferrero, R., Marilli, E., & Catalano, S. 2000, A&A, 364, 179
Freire Ferrero, R., Gouttebroze, P., Catalano, S., Marilli, E., Bruhweiler, F., Kondo, Y., van der Hucht, K., & Talavera, A. 1995, ApJ, 439, 1011
García López, R. J., Rebolo, R., Backman, J. E., & McKeith, C. D. 1993, A&A, 273, 482
Gray, D. F. 1988, Lectures on Spectral-Line Analysis, F, G, and K Stars (Arva: The Publisher)
Gray, D. F. 1992, The Observation and Analysis of Stellar Photospheres (Cambridge: Cambridge Univ. Press)
Gray, R. O., & Corbally, C. J. 1994, AJ, 107, 742
Gray, R. O., Corbally, C. J., Garrison, R. F., McFadden, M. T., & Robinson, P. E. 2003, AJ, 126, 2048
Gray, R. O., & Garrison,, 69, 301
Gray, R. O., Napier, M. G., & Winkler, L. I. 2001, AJ, 121, 2148
Grevesse, N., & Sauval, A. J. 1998, Space Sci. Rev., 85, 161
Hauck, B., & Mermilliod, M. 1998, A&AS, 129, 431
King, J. R., Villarreal, A. R., Soderblom, D. R., Gulliver, A. F., & Adelman, S. J. 2003, AJ, 125, 1980
Kraft, R. P. 1967, ApJ, 148, 129
Krisciunas, K., Griffin, R. F., Guinan, E. F., Luedeke, K. D., & McCook, G. P. 1995, MNRAS, 273, 662
Kurucz, R. L. 1992, in IAU Symp. 149, The Stellar Populations of Galaxies, ed. B. Barbuy & A. Renzini (Dordrecht: Kluwer), 225
Landman, D. A. 1981, ApJ, 244, 345
Landsman, W., & Simon, T. 1993, ApJ, 408, 305
Lundström, I., Ardeberg, A., Maurice, E., & Lindgren, H. 1991, A&A, 91, 199
McAlister, H. A., Hartkopf, W. I., & Mason, B. D. 1992, AJ, 104, 1961
Moon, T. T. 1984, MNRAS, 211, 21P
Napiwotzki, R., Schoenberner, D., & Wenske, V. 1993, A&A, 268, 653
Narain, U., & Ulmschneider, P. 1996, Space Sci. Rev., 75, 453
Neff, J. E., & Simon, T. 2008, ApJ, 685, 478
Nidever, D. L., Marcy, G. W., Butler, R. P., Fischer, D. A., & Vogt, S. S. 2002, ApJS, 141, 503
Niehaus, R. J., & Scarfe, C. D. 1970, PASP, 82, 1111
Nordström, B., et al. 2004, A&A, 418, 989
Press, W. H., Flannery, B. P., Teukolsky, S. A., & Vetterling, W. T. 2000, Numerical Recipes in C, (Cambridge: Cambridge Univ. Press)
Rachford, B. L. 1997, ApJ, 486, 994
Rachford, B. L. 1998, ApJ, 505, 255
Rachford, B. L. 2000, MNRAS, 315, 24
Schmitt, J. H. M. M., Golub, L., Harnden, F. R., Maxson, C. W., Rosner, R., & Vaiana, G. S. 1985, ApJ, 290, 307

Simon, T., & Drake, S. A. 1989, ApJ, 346, 303
Simon, T., & Landsman, W. 1991, ApJ, 380, 200
Soderblom, D. R., & Mayor, M. 1993, AJ, 105, 226
Steffen, M. 1985, A&AS, 59, 403
Teresova, T. N. 2005, Astrophysics, 48, 465
Thevenin, F. 1990, A&AS, 82, 179
van Belle, G. T., Ciardi, D. R., Thompson, R. R., Akeson, R. L., & Lada, E. A. 2001, ApJ, 559, 1155
Varenne, O., & Monier, R. 1999, A&A, 351, 247
Wolff, S. C., Boesgaard, A. M., & Simon, T. 1986, ApJ, 310, 360
Wolff, S. C., & Simon, T. 1997, PASP, 109, 759
Woolley, R. v. d. R. 1970, R. Obs. Ann., 5, 227